

# Numbers Matter: The Role of Cell Dose in the Treatment of Osteosarcoma Using Mesenchymal Stromal Cells as Cellular Vehicles

Elisa Martella, Barbara Dozza, Claudia Ferroni, Chiara Bellotti, Clement Osuru Obeyok, Matilde Tubertini, Andrea Guerrini, Marco Ballestri, Marta Columbaro, Ilse Manet, Marco Gambarotti, Lucia Martini, Milena Fini, Luca Cevolani, Davide Maria Donati, Enrico Lucarelli, Greta Varchi,\* and Serena Duchi\*

A promising approach enhancing osteosarcoma (OS) prognosis involves the combination of various techniques, such as chemo- and photodynamic therapy, delivered through nanocarriers for synergistic cell death. Among the potential candidates for improving drug accumulation at the tumor site, mesenchymal stromal cells (MSCs) exhibit a significant advantage due to their tumor-homing ability and intracellular drug retention. This study evaluates the efficacy of chemo-releasing and photoactive bimodal nanoparticles, kPCe6 NPs, delivered via MSCs. In vitro analyses show that cells internalize and retain kPCe6 NPs in a dose-dependent manner and that kPCe6-loaded cells induce massive tumor cell death in a tridimensional tumor model. Results from an in vivo orthotopic OS murine model show negligible tumor cell death upon peritumoral administration of two doses containing  $10^6$  loaded cells. To gain insight into this observation, this work investigates the role of cell dose in treatment efficacy. The results indicate that achieving a tumor reduction higher than 90% requires a substantial number of loaded cells, approximately 35% of the entire tumor mass, highlighting the criticality of the cell dose for the success of this therapeutic approach and its potential impact on clinical translation in OS patients, particularly when the number of tumor cells is limited.


## 1. Introduction

Osteosarcoma (OS) is the most common type of bone tumor and is characterized by varying degrees of malignancy.<sup>[1,2]</sup> High-grade OS (HGOS) is the most aggressive subtype with a favorable outcome only in 60–65% of patients who are under 40 years old with localized and nonmetastatic disease at clinical presentation.<sup>[3,4]</sup> Despite this subset of HGOS, patients may benefit from multiagents neoadjuvant chemotherapy;<sup>[5,6]</sup> the suboptimal response to drugs leads to tumor recurrence, which, in most cases, progresses to the development of lung metastases within the first 24–36 months from diagnosis.<sup>[7]</sup>

One option to improve OS treatment is the use of nanoformulations combining different therapeutic techniques, such as chemo- and photodynamic therapy (PDT), triggering different cellular responses and inducing synergistic cell death. Despite the modest anticancer effectiveness of Taxol,

E. Martella, C. Ferroni, C. Osuru Obeyok, M. Tubertini, A. Guerrini, M. Ballestri, I. Manet, G. Varchi, S. Duchi  
Institute for the Organic Synthesis and Photoreactivity (ISOF)  
National Research Council (CNR)  
Via Piero Gobetti 101, Bologna 40129, Italy  
E-mail: greta.varchi@isof.cnr.it; sduchi@unimelb.edu.au  
B. Dozza, D. M. Donati  
Department of Biomedical and Neuromotor Sciences (DIBINEM)  
Alma Mater Studiorum University of Bologna  
Via di Barbiano 1/10, Bologna 40136, Italy

C. Bellotti, E. Lucarelli  
Osteoncologia  
Sarcomi dell'osso e dei tessuti molli, e Terapie Innovative  
IRCCS Istituto Ortopedico Rizzoli  
Via di Barbiano 1/10, Bologna 40136, Italy  
M. Columbaro  
Electron Microscopy Platform  
IRCCS Istituto Ortopedico Rizzoli  
Via di Barbiano 1/10, Bologna 40136, Italy  
M. Gambarotti  
Department of Pathology  
IRCCS Istituto Ortopedico Rizzoli  
Via di Barbiano 1/10, Bologna 40136, Italy  
L. Martini  
Scienze e Tecnologie Chirurgiche  
IRCCS Istituto Ortopedico Rizzoli  
Via di Barbiano 1/10, Bologna 40136, Italy

 The ORCID identification number(s) for the author(s) of this article can be found under <https://doi.org/10.1002/adtp.202300045>

© 2023 The Authors. Advanced Therapeutics published by Wiley-VCH GmbH. This is an open access article under the terms of the Creative Commons Attribution-NonCommercial License, which permits use, distribution and reproduction in any medium, provided the original work is properly cited and is not used for commercial purposes.

DOI: 10.1002/adtp.202300045

i.e., the solvent-based formulation of paclitaxel, in OS patients,<sup>[8]</sup> the albumin-based paclitaxel nanof ormulation, e.g., Abraxane, demonstrated superior clinical safety and efficacy in different solid tumors, thus unlocking novel therapeutic options for OS treatment.<sup>[9]</sup> A phase II clinical trial is currently ongoing to assess whether the combination of Abraxane with gemcitabine can prevent the formation or growth of tumors in patients with relapsed or refractory OS and other solid tumors (<http://clinicaltrials.gov/show/NCT02945800>) (Figure 1).

Driven by these concepts, we generated a bimodal system combining chemo and photo therapies within biodegradable keratin nanocarriers.<sup>[10]</sup> This nanof ormulation, loaded with both paclitaxel (PTX) and Chlorin e6 (Ce6) (chemo-photo NPs, Figure 1) induced a 78% tumor reduction in a preclinical orthotopic OS model<sup>[11]</sup> when injected peritumorally. However, this study highlighted that this bimodal strategy might be insufficient to retain the drugs at the tumor site for more than 24 h after the administration and that the photosensitizer rapidly diffuses into the surrounding healthy tissues, probably due to the lack of a retention system, inducing an undesirable level of inflammation.

In recent years, numerous cancer-targeting methods have emerged, including passively targeted nanocarriers and actively targeted therapeutics, e.g., antibody-drug conjugates (ADCs). However, the primary mechanism of their tumor accumulation relies on the enhanced permeability and retention (EPR) effect for nanocarriers and the selective recognition of surface receptors for ADCs. Nevertheless, the abundant stroma in some tumor types, such as OS, significantly impedes the uptake of nanocarriers and the binding of ADCs.<sup>[12]</sup> Consequently, there is a growing interest in exploring cancer-targeting approaches that are independent of these pathways and can effectively penetrate the tumor stroma.

Among these options, the use of cellular vehicles such as autologous cells isolated from different tissues, including mesenchymal stromal cells (MSCs), has gathered increasing attention<sup>[12–14]</sup> to improve the drug targeting and retention at the tumor site while reducing the side effects due to uncontrolled drug diffusion. Pioneered by Studeny,<sup>[15]</sup> MSCs have emerged as promising carriers of drugs, reducing their systemic toxicity and multi-drug resistance (MDR) by controlling their release to specific tissues thanks to the MSCs' tumor homing ability.<sup>[16–18]</sup> More than a hundred papers have been published where the authors leveraged the tropism of MSCs toward tumor stroma for the targeted delivery of a diverse range of agents, enabling the selective eradication of tumor cells. This strategy has been used also to target bone sarco-

mas; for example, Grisendi and co-authors used MSCs to deliver tumor necrosis factor-related apoptosis-inducing ligand (MSCs-TRAIL) to different sarcoma histotypes. When 10<sup>6</sup> MSCs-TRAIL were injected into a xenotransplants model of Ewing sarcoma, MSCs-TRAIL persisted within the stroma causing significant tumor apoptosis versus control groups.<sup>[19]</sup> In another study, Qiao and co-authors used MSCs transfected with adenoviruses carrying the OPG gene (MSCs-OPG) and injected 10<sup>6</sup> MSCs-OPG to treat athymic nude mice (nu/nu) bearing OS. Their results showed that infected MSCs-OPG labeled with red fluorescent protein (RFP) could migrate to tumor sites and express the OPG protein. The treatment by MSCs-OPG reduced the tumor growth and inhibited bone destruction *in vivo*.<sup>[20]</sup>

We therefore explored whether MSCs could efficiently act as cellular vehicles of our photoactive nanoparticles (photo-NPs@MSCs, Figure 1), improving their tumor stroma retention and decreasing the extent of side effects. In our first study, photo-NPs@MSCs showed distribution and retention inside the lysosomal compartments for several days, thus allowing PDT to be repeated multiple times *in vitro* with no need of additional administration.<sup>[16]</sup> In a more recent study, we used a subcutaneous preclinical murine OS model, demonstrating that intratumorally injected photo-NPs are retained within the tumor area when delivered via MSCs<sup>[21]</sup> with consequent significant tumor reduction. Evident skin toxicity was observed only in the photo-NPs-treated groups, indicating that MSCs allow better accumulation in the tumor while reducing the extent of side effects.

In the current study, we aim to test the effectiveness of our chemo-photo bimodal NPs system delivered via MSCs, e.g., kPCe6@MSCs (chemo-photo NPs@MSCs, Figure 1), *in vitro* and in an orthotopic murine OS model. Relying on a specifically devised tridimensional OS model, we finally investigated the role of the cell dose in the *in vivo* therapeutic response.

## 2. Results and Discussion

### 2.1. Cells Source: MSCs Characterization

To investigate whether MSCs can be effective carriers of kPCe6 NPs<sup>[11]</sup> for the *in vivo* treatment of OS while also envisioning a clinical translation of our combined approach, we used strictly defined procedures for bone marrow (BM) withdrawal,<sup>[22]</sup> MSCs isolation, and expansion<sup>[21,23]</sup> to establish the best MSCs lines among five donor patients. In agreement with the International Society for Cellular Therapy (ISCT) that set the minimal criteria to define multipotent MSCs,<sup>[24–26]</sup> the five cell lines were tested for their plastic adherence, positive expression of CD90 and CD73, and negative expression of hematopoietic and endothelial markers CD14, CD31, CD34, and CD45. Furthermore, the *in vitro* differentiation into adipocyte, chondrocyte, and osteoblast lineages was determined. The results shown in Figure 2 report the data of proliferation (growth curves, Figure 2A), clonogenic potential (before and after density gradient separation, Figure 2B), immunophenotype (Figure 2C), and multilineage potential (Figure 2D–F). A score system was then applied on the collected data to rank the cell lines according to their computed performance. The MSCs line 266 obtained the highest outcome with a cumulative score of 59 and therefore was selected for our study (Table S1, Supporting Information). This quantitative

M. Fini  
Scientific Director  
IRCCS Istituto Ortopedico Rizzoli  
Via di Barbiano 1/10, Bologna 40136, Italy  
L. Cevalani, D. M. Donati  
Unit of 3rd Orthopaedic and Traumatologic Clinic Prevalently Oncologic  
IRCCS Istituto Ortopedico Rizzoli  
Via Pupilli 1, Bologna 40136, Italy  
S. Duchi  
Department of Surgery-ACMD  
St. Vincent's Hospital Melbourne  
University of Melbourne  
29 Regent Street, Fitzroy, VIC 3065, Australia

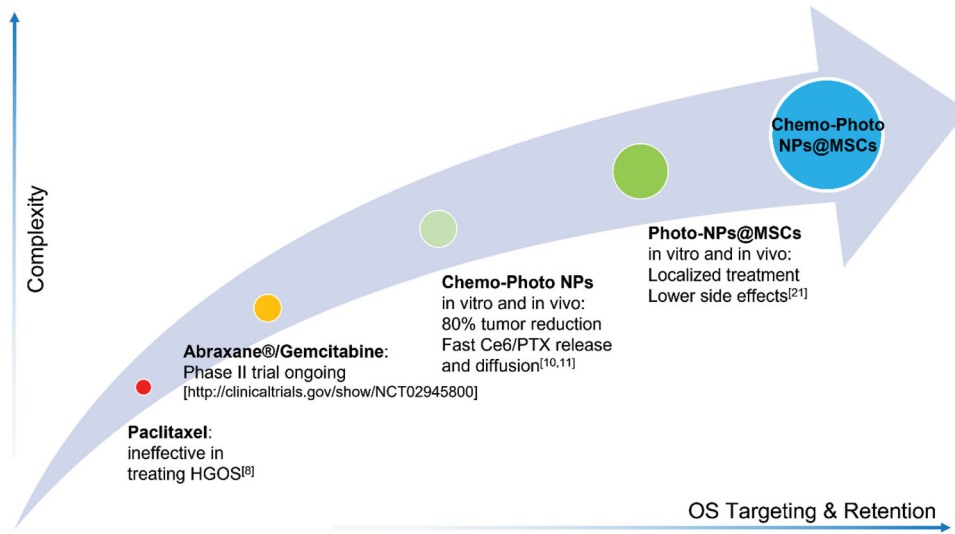


**Figure 1.** Graphical representation of the rationale and the results that steered our strategy over time leading to the current work.

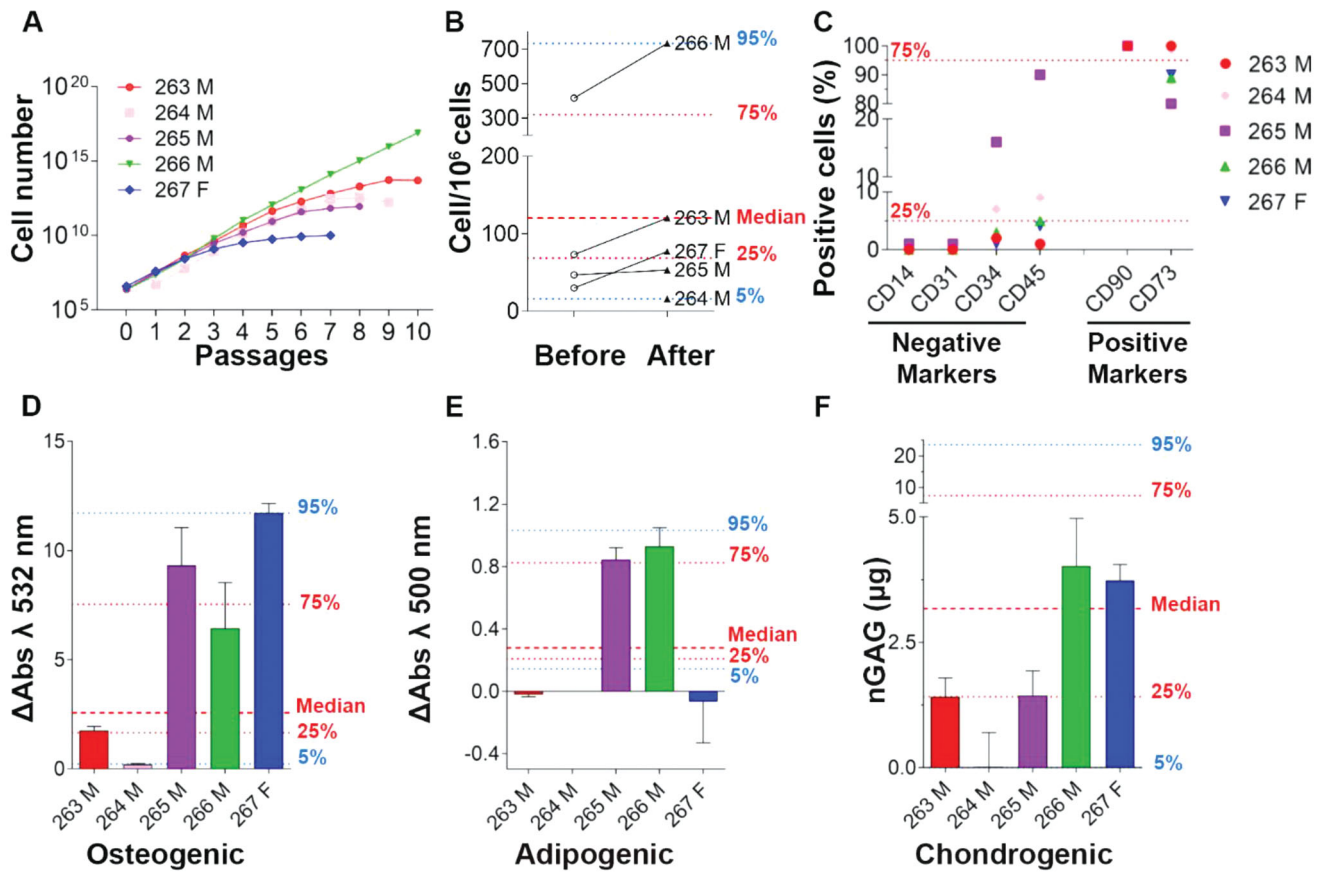


**Figure 2.** MSC characterization. The graphs show data related to the characterization analyses performed on five different MSCs lines. In all graphs, the number of the cell line and the patient gender (M/F) are reported. A) Growth curve expansion (cell number/passages). B) Colony forming unit (CFU) assay to evaluate cell concentration before and after Ficoll plaque' separation. C) immunophenotype; D–F) multilineage differentiation capacity: osteogenic, adipogenic, and chondrogenic differentiation, respectively. In graphs B,D–F, in blue 5th and 95th percentiles are reported, while in red 25th, 75th percentiles, and median, obtained from the analyses of characterization data from our MSCs bank are reported. The CD90 expression is comparable for all the cell lines analyzed.

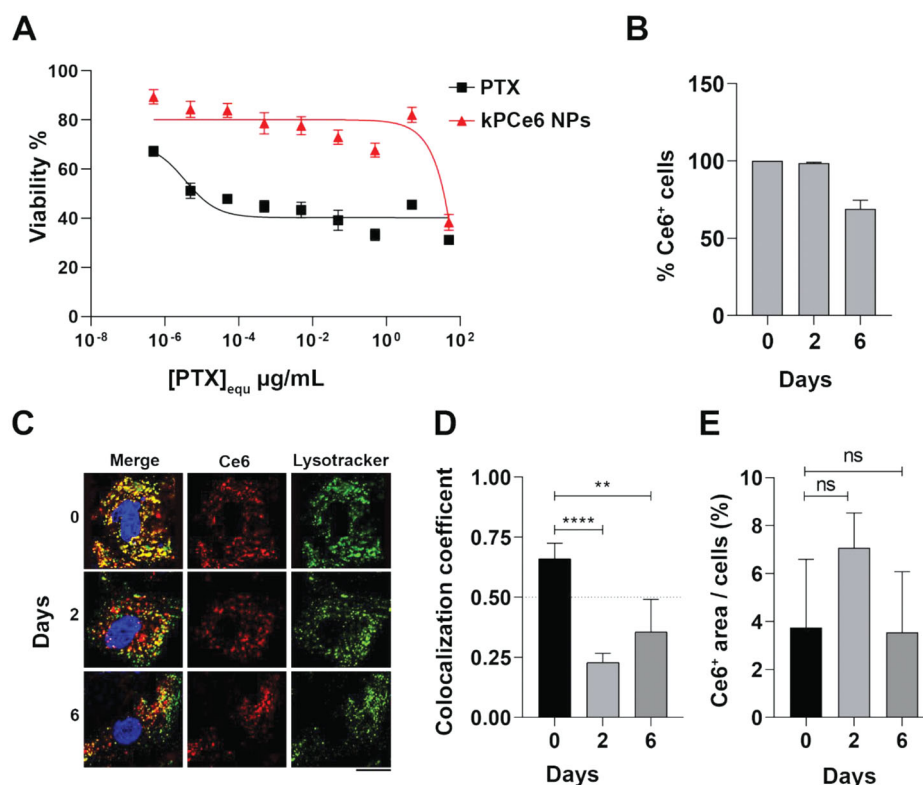


**Figure 3.** Cell loading and retention: characterization of kPCe6 NPs internalization into MSCs. A) IC<sub>50</sub> evaluation on MSCs after exposure to PTX alone (black square) or kPCe6 NPs (red triangle). B) The bar graph shows the quantification over time of Ce6 positive cells normalized to the total number of analyzed cells at time 0 (the end of 24 h loading phase), 2 and 6 days after. C) Representative confocal images of MSCs loaded for 24 h with kPCe6 NPs PT at [PTX]<sub>equ</sub> = 5 µg mL<sup>-1</sup> and incubated for 10 min with Lysotracker DND-26 (green) and Hoechst (blue). The fluorescence of Ce6 is shown in red, while the yellow color corresponds to the overlapping signals between Lysotracker and Ce6 in the merge column. The acquisition was performed at time 0 (the end of 24 h loading phase), 2, and 6 days after. Scale bar 20 µm. D) The bar graph shows the Pearson colocalization coefficient (summarized signal) calculated on Ce6 over Lysotracker signals in kPCe6@MSCs at time 0 (the end of loading phase), 2, and 6 days after. Results were analyzed using an unpaired *t*-test and they were statistically significant at *p* values < 0.05. (\**p*-values < 0.05, \*\**p*-values < 0.01, \*\*\**p*-values < 0.001, \*\*\*\**p*-values < 0.0001). Values > 0.5 (dotted line) indicate a high probability that pixels of both channels are overlaid. E) The bar graph shows the quantification of intracellular Ce6 signal in kPCe6@MSC at time 0 (the end of loading phase), 2 and 6 days after normalized for cell area. All statistical analyses were performed with GraphPad Prism 8 software (GraphPad; San Diego, CA, USA).

selection, based on the comparison with the statistical parameters obtained from 28 MSCs lines isolated and cultured with the same standardized protocol, had the purpose to assess the three general quality criteria required by FDA and EMA,<sup>[27]</sup> e.g., identity, purity, and proliferative capacity against internal and published reference standards, setting the ground for the development of GMP grade production and clinical translation.

## 2.2. Cell Loading and Retention: Characterization of Keratin NPs Internalization Into MSCs

In the present study, we used MSCs as cellular vehicles of biodegradable keratin nanocarriers, loaded with both PTX and Chlorin e6 (Ce6), namely kPCe6 NPs, whose physical and chemical properties had been extensively investigated in our previous works.<sup>[10,11]</sup> A key parameter for the success of the proposed approach is the MSCs' loading and retention capability. To establish the cells' culture conditions allowing the optimal kPCe6 NPs uptake, different loading time and culture media were tested and, to quantify the efficiency of intracellular

internalization,<sup>[28]</sup> the intrinsic fluorescence of Ce6 was used as a readout. Considering that serum proteins play an important role in NPs internalization, different loading time and culture media formulations were tested. An optimization study allowed to establish 24 h as the best-performing time (data not shown) to obtain the highest kPCe6 NPs cell uptake and retention. To determine the most suitable cell culture medium for the dilution and kPCe6 NPs uptake, two culture conditions were tested,  $\alpha$ -MEM supplemented with either 20% FBS or 0.2% BSA (Figure S1, Supporting Information). Our results demonstrated a significant increase in kPCe6 NPs cellular internalization when using 0.2% BSA with respect to cell culture medium supplemented with 20% FBS (Figure S1, Supporting Information). Therefore, the internalization step in MSCs for the whole study was performed under 0.2% BSA condition.

Cellular viability was measured to verify that the NPs internalization did not significantly alter the cells' metabolic activity. Our findings indicate that the viability of cells exposed to increasing concentrations of PTX loaded into kPCe6 NPs was less affected compared to cells exposed to the same concentration of the free drug (Figure 3A). For kPCe6 NPs, a 40% viability reduction was

observed only at the highest tested PTX concentration ( $[PTX]_{\text{equ}}: 50 \mu\text{g mL}^{-1}$ ).

Based on these results, we exposed MSCs to a concentration of  $[PTX]_{\text{equ}} 5 \mu\text{g mL}^{-1}$  (corresponding to  $[kPCe6] = 38.5 \mu\text{g mL}^{-1}$  and  $[Ce6] = 2.5 \mu\text{g mL}^{-1}$ ) in all the following experiments.

The ability of MSCs to retain the NPs over time was quantitatively estimated by intracellular fluorescence measurement of Ce6, demonstrating that 100% of Ce6 was retained up to 2 days after loading, and 75% was still present at day 6 (Figure 3B). Confocal imaging confirmed these results revealing that the Ce6 signal significantly colocalized with the LysoTracker signal arranged in vesicle-like structures diffused around the nuclei and in the cytosol (Figure 3C), as also corroborated by transmission electron microscopy (TEM) analysis (Figure S2, Supporting Information). The quantitative analysis of overlapping red and green channel pixels (Ce6 over LysoTracker, respectively), as verified by the Pearson coefficient (Figure 3D), indicated a peak of colocalization at the end of the loading phase (24 h), which decreased after 2 days but remained constant up to 6 days.

The reduced colocalization over time could be ascribed to a reshuffling of the NPs inside the different intracellular compartments,<sup>[29]</sup> or to the enzymatic degradation of the NPs inside the lysosomes (LysoTracker positive vesicles) with consequent release of Ce6 and PTX inside the cells, as already reported for other protein-based nanocarriers.<sup>[30]</sup> Release of Ce6 in the acidic organelles can induce a decrease of Ce6 fluorescence intensity signals due to the lower quantum yield of Ce6 fluorescence at lower pH.<sup>[31]</sup> Furthermore, the quantification of the cell area endowed by the Ce6 signal over time shown in Figure 3E confirms its intracellular retention, and the signal's oscillations may reflect the trafficking of Ce6 inside the cell and/or its release from the keratin over time.

Overall, these results confirm the role of MSCs to sequester the NPs inside their endocytic compartments delaying the undesired diffusion of the drugs and improving the retention of the therapeutic agents at the tumor site. The utilization of NPs for loading chemotherapeutic drugs effectively protects MSCs from direct interaction with toxic drugs, and formation of efflux transporters on MSCs. They create a "cellular drug depot" releasing the drug over a period longer than 24 h.<sup>[32]</sup>

### 2.3. Cell Migration Performance: Impact of kPCe6 NPs on MSCs Motility

Loading drugs into MSCs can potentially decrease their migratory capacity. Therefore, it is essential to carefully consider this effect when establishing the optimal number of cells to be used and selecting the most suitable administration modality. For instance, intravenous versus intra- or peritumoral administration routes can impact the ability of cells to reach the tumor mass.

Therefore, the migration property of kPCe6@MSCs was firstly investigated through the Transwell assay, testing two distinct chemoattractant media: the MG-63 conditioned medium (CM) and the cell culture medium supplemented with 20% FBS, widely reported as a positive control for cells migration.<sup>[33]</sup> Results show that, compared to unloaded MSCs, kPCe6@MSCs preserved a 50% migration ability upon NPs internalization (Figure 4A,B). Importantly, kPCe6@MSCs are still able to recognize the stimuli released by the tumor cells and preferentially migrate toward the

tumor-released chemoattractant molecules (Figure S3, Supporting Information). Overall, these data confirm the tumor tropism of MSCs toward OS cells.

To further investigate the cellular migration upon NPs loading, a scratch wound-healing assay was performed on kPCe6@MSCs and compared to unloaded MSCs (Figure 4C). The results highlight that at 48 h postscratch, the kPCe6@MSCs closed 50% of the wound ( $p = 0.0276$ ), while unloaded MSCs covered the entire area within the same time frame ( $8 \pm 2\%$  remaining area after 48 h, Figure 3D). This result supports that, despite being partially diminished, kPCe6@MSC migration capability is preserved.

### 2.4. OS in Vitro Model: Efficacy of kPCe6@MSCs in 3D Osteosarcoma Model

To investigate the in vitro efficacy of our MSCs-based system, we generated a 3D scaffold-free OS tumor model (3D-OSM) coculturing MG-63 OS cells and kPCe6@MSCs (Figure 5A).

The MG-63 cell line was selected based on our previous findings on three different OS cells (MG-63, SaOS-2, and U-2 OS), indicating that only MG-63 are capable of developing reproducible, homogeneous and viable three-dimensional (3D) scaffold-free tumor spheroids.<sup>[21]</sup> To investigate the effect of the kPCe6@MSCs/MG-63 ratio on cell death and eventually select the best-performing conditions for in vivo studies, we used two different kPCe6@MSCs doses keeping fixed the number of tumor cells: 3170 and 1360 kPCe6@MSCs versus 9500 MG-63 cells, respectively.

To verify that the starting metabolic activity baseline was the same in all tested settings, regardless of the different cellular compositions of the 3D-OSM model, we measured the ATP content (Figure S4A, Supporting Information). Our results show no significant difference between the two MSCs doses tested (3160 and 1370, respectively) (Figure S4A, Supporting Information –PDT). TEM and ATP content analyses also confirmed that exposure to light irradiation does not alter cell metabolism on the 3D-OSM composed of unloaded MSCs at all tested conditions (Figure S4, Supporting Information). These controls were essential to unambiguously measure the tumor cell death upon our chemo and photo therapeutic treatment.

PTX efficacy was preliminarily evaluated by measuring the cytotoxicity of kPCe6@MSCs in the dark up to 5 days after 3D-OSM formation, at the two different kPCe6@MSCs concentrations (3170 and 1360, respectively). The results show a 50–60% cell viability reduction up to 4 days in both cases (Figure S5, Supporting Information), indicating that light irradiation could be suitably performed at this timepoint. A timeline of the assay and the conditions tested are summarized in Figure 5A.

The OS cells and MSCs death was analyzed by ATP quantification on 3D-OSM 24 h after light irradiation (LED light at  $667 \pm 3 \text{ nm}$  for 10 min, light intensity:  $198 \text{ mW cm}^{-2}$ ; fluence:  $120 \text{ J cm}^{-2}$ ) or keeping the samples in the dark. In nonirradiated samples (Figure 5B –PDT), we measured a 40% and a 20% reduction in cell viability for the 3170/9500 and the 1360/9500 ratio, respectively. The combination of chemo- and PDT induced 90% and 80% cell death at the two ratios tested, respectively (Figure 5B+PDT). Confocal microscopy (Figure 5C) and TEM images (Figure 5D) highlight the massive consequent necrosis

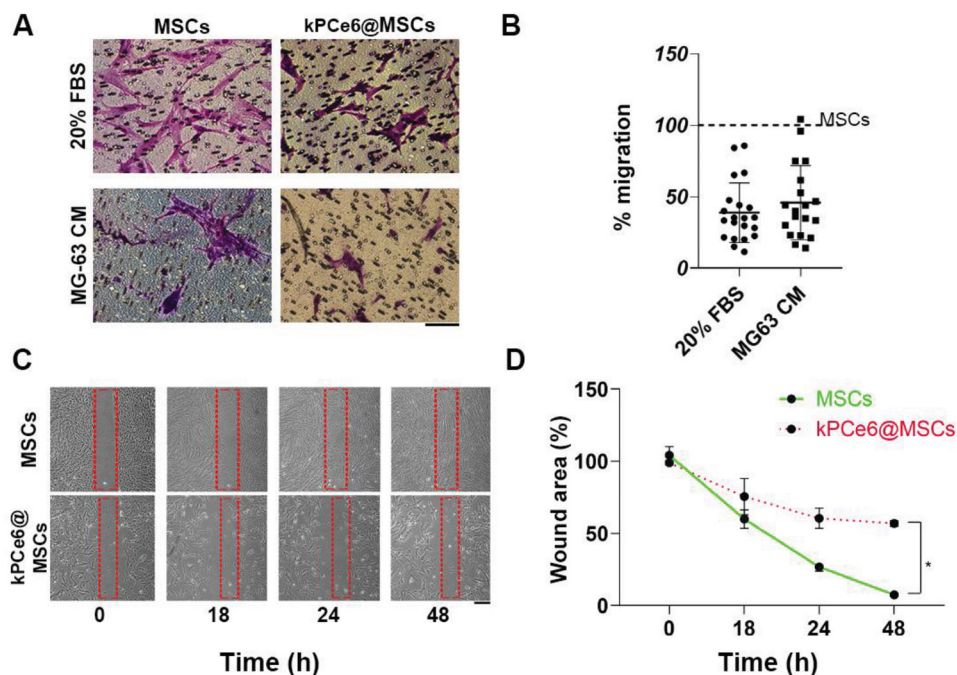


**Figure 4.** Impact of kPCe6 NPs on MSCs migration. A) Representative images of Transwell assay performed with kPCe6@MSCs at  $[PTX]_{equ} 5 \mu\text{g mL}^{-1}$ . The assay was performed in two distinct conditions, medium supplemented with 20% FBS or MG-63 conditioned medium (CM), both used as chemoattractant. Scale bar 50  $\mu\text{m}$ . B) The graph reports the quantification of the cell migration obtained from cell counting in 10 random fields of each Transwell basket compared to unloaded cells ( $N = 3$  independent experiments,  $n = 3$  replicates). C) Representative images of scratch assay test performed on kPCe6@MSCs and MSCs observed at the indicated time points. Scale bar 50  $\mu\text{m}$ . D) The graph reports the quantification of wound area (mean  $\pm$  SD) from the images of the scratch assay ( $N = 3$  independent experiments,  $n = 3$  replicates) normalized to control group. Results were analyzed using an unpaired  $t$ -test and they were statistically significant at  $p$  values  $< 0.05$  ( $^*p$ -values  $< 0.05$ ). All statistical analyses were performed with GraphPad Prism 8 software (GraphPad).

inside the 3D-OSM (red cells in Figure 5C +PDT and yellow asterisk, Figure 5D +PDT). These findings are especially significant when considering the potential impact of MSCs on tumor progression.<sup>[34]</sup> Indeed, our approach successfully eradicates both MSCs and tumor cells upon light irradiation, effectively eliminating any potential contribution of MSCs to tumor growth.

## 2.5. Preclinical Evaluation: Efficacy of kPCe6@MSCs in Orthotopic Murine Osteosarcoma Model

Given the rarity and significant heterogeneity of OS, along with the challenges associated with recruiting an adequate patient population for clinical trials,<sup>[35]</sup> it becomes essential to optimize preclinical research models.

Although subcutaneous OS tumors are widely diffused due to their feasibility, reproducibility, and ease of monitoring, we reasoned that an orthotopic OS murine model, despite more challenging, could have provided a more physiological indication in view of clinical translation.

Therefore, the *in vivo* experimentation was performed in an OS orthotopic murine model previously optimized and characterized by our team and that well recapitulates the hallmarks of the human OS.<sup>[11]</sup> We then established the following parameters: cells number, cells administration route, and treatment schedule.

The inclusion of live cells increases the complexity of the treatment from the perspective of the “dose” of cells to be injected.

Several preclinical studies have shown that the relationship between cell dose and clinical benefits are not always linear.<sup>[36–38]</sup> Therefore, we decided to start from a number of cells ( $10^6$  loaded MSCs) previously used by our team<sup>[21]</sup> and corroborated by other authors in the same field.<sup>[19,20]</sup>

Regarding the administration route, published data report two options: systemic and local. Unless properly engineered, MSCs administered through intravenous route are mainly retained into the lungs,<sup>[39,40]</sup> whereas other types of systemic administration, such as intra-arterial or intraportal, require invasive surgical interventions and have proved effective in treating only tumors of first-pass organs.<sup>[12]</sup> Therefore, we opted for a local peritumoral injection, 5 weeks after intratibial tumor cells inoculation.

To establish the treatment schedule, we investigated the Ce6 localization by means of confocal imaging exploiting both its fluorescence intensity and lifetime in animals euthanized immediately after (0 h) or 48 h after cells injection (Figure 6). Confocal images highlighted that kPCe6@MSCs retain the nanoparticles even after 48 h from the local injection (Figure 6A). Spectral imaging was also performed to discriminate Ce6 signal from tissue autofluorescence, showing that at both time points, the signal observed is specific for Ce6 (Figure 6B). Moreover, taking advantage of the high sensitivity of the fluorophore to the local environment, fluorescence lifetime imaging (FLIM) analysis on Ce6 was performed (Figure 6C). The average fluorescence lifetime did not change with the exposure time, confirming the intracellular retention of NPs in similar organelles at both time

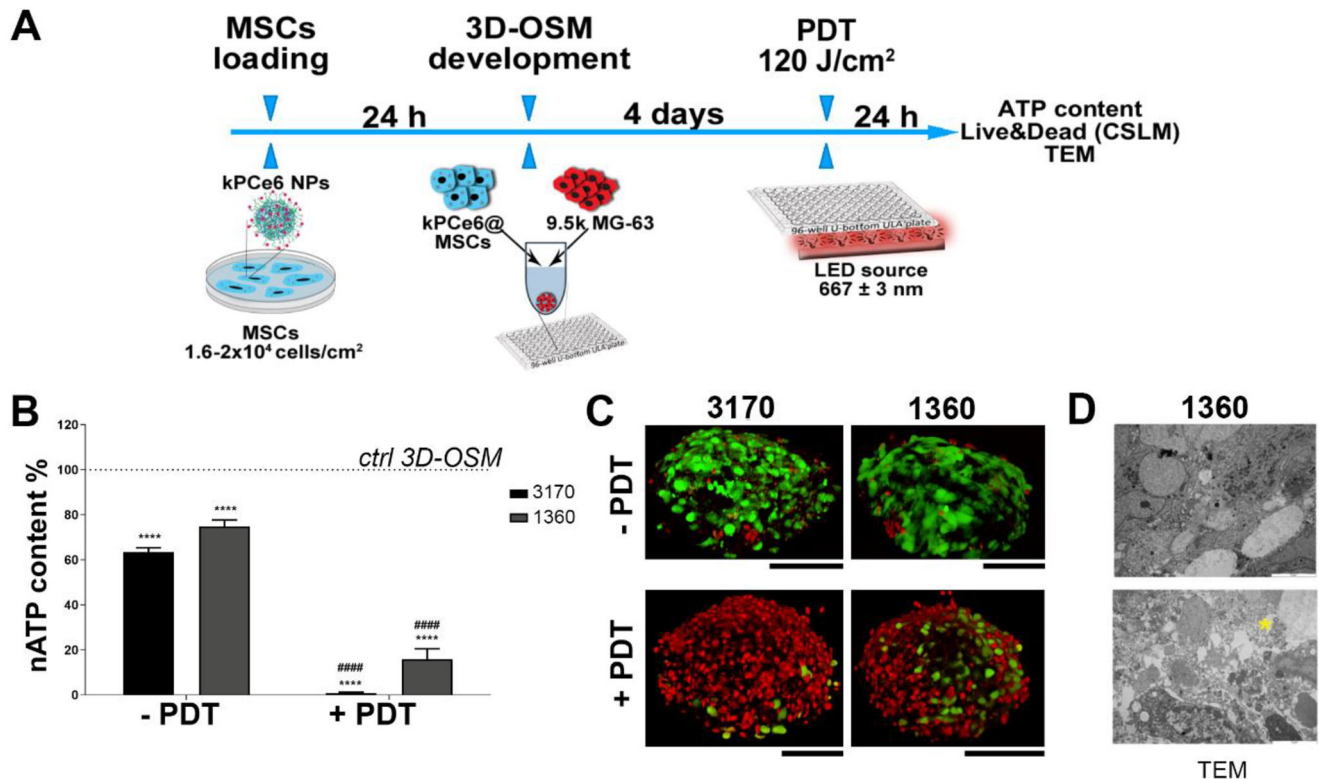


**Figure 5.** Efficacy of kPCe6@MSCs in OS 3D -OSM. A) Schematic representation of the workflow of 3D-OSM generated with different amount of kPCe6@MSCs, keeping fixed the number of MG-63. B) The graph shows data obtained by Cell Titer Glo assay performed 24 h after irradiation (–/+PDT) at two different kPCe6@MSCs doses and MG-63 cells. The results are normalized to the corresponding 3D-OSM generated with unloaded MSCs and nonirradiated. Data are expressed as mean ± SD ( $N = 6$  and  $n = 4$ ) and statistical analysis has been performed by GraphPad Prism software using the 2-way ANOVA test, and Tukey's multiple comparison test as a post-test. Results were considered statistically significant at  $p$  values < 0.05. (\*  $p$ -values < 0.05, \*\*  $p$ -values < 0.01, \*\*\*  $p$ -values < 0.001, and \*\*\*\*  $p$ -values < 0.0001). Data compared to respective unloaded MSCs are reported as \*, while the # indicate the statistical analysis performed comparing the corresponding ratio groups –/+PDT. C) Representative confocal images of Live&Dead staining (green Calcein AM staining of live cells and red EthD-1 staining of dead cells' nuclei) of nonirradiated (–PDT) and irradiated (+PDT) 3D-OSM at different kPCe6@MSCs doses. Scale bar 100  $\mu$ m. D) Representative TEM images of nonirradiated (–PDT) and irradiated (+PDT) 3D-OSM at 1360 kPCe6@MSCs dose, where yellow asterisk highlights necrosis. Scale bar 5  $\mu$ m.

points evaluated (Table S2, Supporting Information). In addition, the Ce6 fluorescence decay afforded almost identical average lifetimes ( $\tau_{av}$ ) for kPCe6 NPs<sup>[11]</sup> (entries 3 and 4, Table S2, Supporting Information) and kPCe6@MSCs (entries 6 and 7, Table S2, Supporting Information), indicating that Ce6 maintain the same properties in comparable environments and that NPs do not undergo significant physical or chemical changes in the observed conditions.

Taking into consideration all of these aspects, the treatment was performed at weeks 5 and 6, inoculating at both time points 10<sup>6</sup> kPCe6@MSCs in the tumor area and exposing half of the animals to light irradiation 48 h later (Figure 7A) by using an in-house designed and manufactured irradiation device.<sup>[11]</sup>

As shown in Figure 7B, OS tumor developed inside the tibia medullar channel, affecting the integrity of the bone and, in some cases, invading the surrounding tissues (such as muscle) like in human patients. During the study, none of the treated animals presented lameness in the hind limbs or worsening of the clinical conditions, indicating that the treatment was better tolerated with respect to the kPCe6 NPs alone which resulted in severe inflammation.<sup>[11]</sup> On the other hand, the quantification

performed on the histological sections of euthanized animals at the end of the treatment (tumor area and number of cells in the tumor area), did not highlight a significant reduction of the tumor size (Figure 7C), as confirmed by the presence of proliferative cells (Ki-67 positive cells) and the absence of apoptotic cells in TUNEL staining (Figure 7D).

Among the factors contributing to this result, we hypothesized that an insufficient number of kPCe6@MSCs were used to treat such a large tumor. To verify this assumption, we used our 3D-OSM to investigate the cell-dose response dependency.

## 2.6. Numbers Matter: Investigation on Cell Dose Response in 3D-OSM

While animal experimentation remains crucial for clinical translation, the use of 3D in vitro models has proved effective for the optimization of several parameters allowing to better define the experimental conditions, such as cell dose.<sup>[41]</sup> Therefore, instead of performing additional trial-and-error in vivo experiments to identify the number of kPCe6@MSCs which could effectively

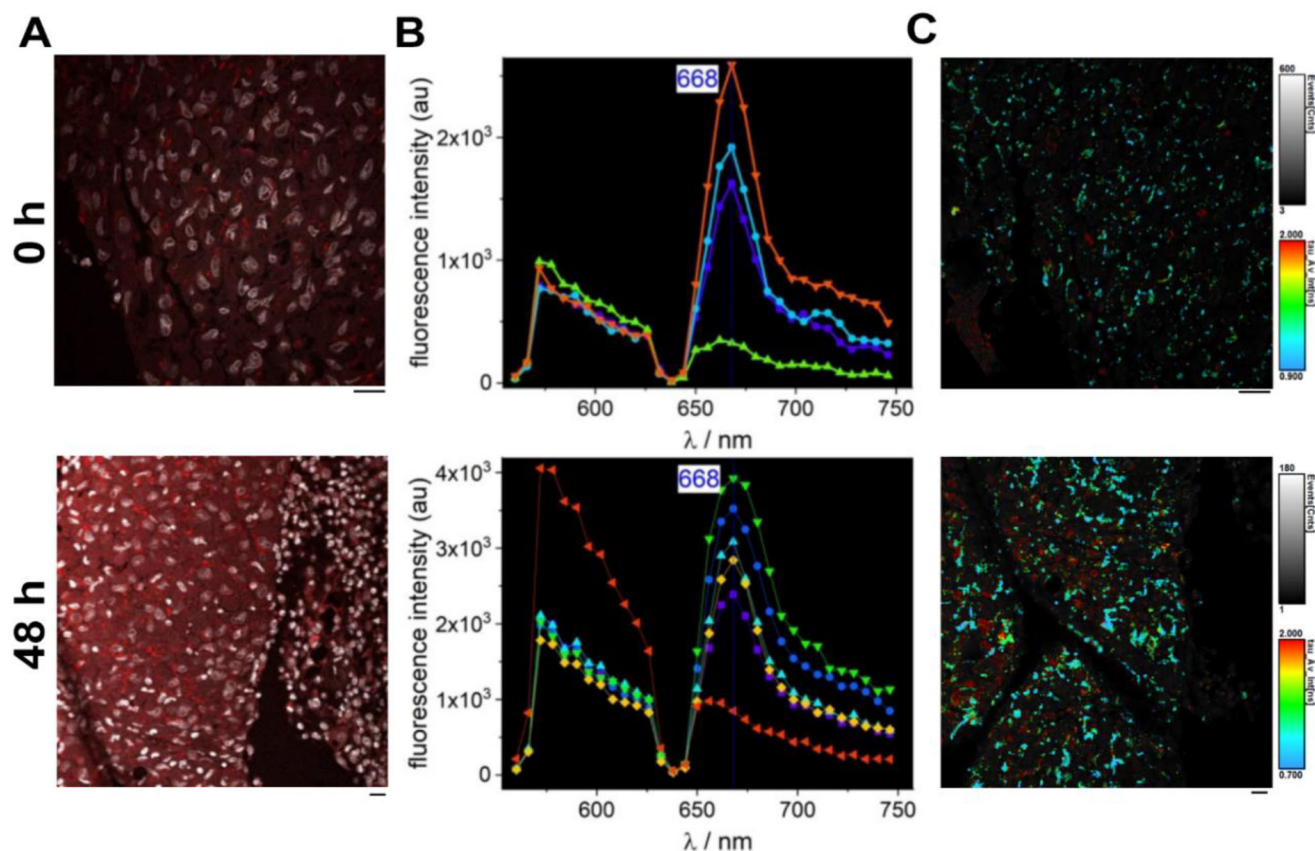


**Figure 6.** Preclinical evaluation: treatment's schedule. A) Representative confocal images of samples from mouse injected with kPCe6@MSCs and euthanized immediately (0 h) or 48 h after treatment: the red signal corresponds to the Ce6 molecule, while nuclei are shown in white. Scale bar 10 μm. B) Representative spectral profiles of different areas identified in the images A) at both times point (0 and 48 h). Samples were excited at 405 nm. Zero intensity at 560 and 640 nm is due to dichroic mirror choice. C) Representative figure of FLIM analysis showing the Ce6 signal distribution in the tissue area right after kPCe6@MSCs inoculation (time 0 h) with the color scale indicating the average lifetime. The blue regions with  $\tau_{av}$  of around 1 ns are indicative of Ce6 while the red coloured regions, characterized by a  $\tau_{av}$  of >2 ns, are indicative of autofluorescence and Hoechst staining in the nuclei. Scale bar 10 μm.

reduce the tumor size, we performed additional experiments on our 3D-OSM model (Figure 5A) to test different cell-dose responses. This valuable information will greatly inform future in vivo studies.

We hypothesized that the 3160/9500 and 1370/9500 kPCe6@MSCs/OS cells ratios assessed in the in vitro 3D-OSM experiment (see §3.4) do not reflect the actual in vivo scenario. To test our hypothesis, we considered a kPCe6@MSCs/OS cells ratios of 630, 500 and 245/9500 and verified their performances in the 3D model.

Our results confirmed that stromal cells have a negligible contribution in ATP content (Figure S6A, Supporting Information) at the selected unloaded MSCs doses, and that at all kPCe6@MSCs doses, the percentage of cell death caused by PTX is insufficient to affect tumor cell viability. A linear decrease was observed when reducing the amount of kPCe6@MSCs (Figure 8A –PDT), highlighting a striking cell dose-efficacy dependency and emphasizing a critical dose below which the amount of PTX vehiculated by MSCs is insufficient to affect tumor cells viability.

Similarly, upon light irradiation (kPCe6@MSCs +PDT, Figure 8A), the reduction of cell viability linearly decreases with

reducing the kPCe6@MSCs dose, reaching a 20% reduction at the lowest dose (245/9500).

The cell viability was further evaluated via confocal imaging performed on the whole 3D-OSMs, either exposed to light irradiation or kept in the dark. Confocal images of Calcein AM/Ethidium homodimer staining confirm a minimal cell death due to PTX activity (red cells) at all doses tested with higher efficacy upon light irradiation (Figure 8B).

To further investigate the effect of PTX and PDT on the 3D-OSM, ultrastructural analysis was performed (-/+ PDT, Figure 8C). TEM observations revealed two different types of cell death in the 3D-OSMs with different kPCe6@MSCs. Compared to controls with unloaded MSCs where cell morphology was not altered (Figure S6B, Supporting Information), in PDT-treated kPCe6@MSCs samples necrosis (asterisks), cytoplasmic swelling, and organelle destruction was observed in all the conditions. Interestingly, irradiated 3D-OSMs revealed the presence of atypical morphological alterations not strictly ascribable to autophagy, apoptosis, or necrosis. An increase of damaged cellular structures characterized by cellular shrinkage, cytoplasmic vacuolization (V), and pyknotic nuclei with clumping of chromatin



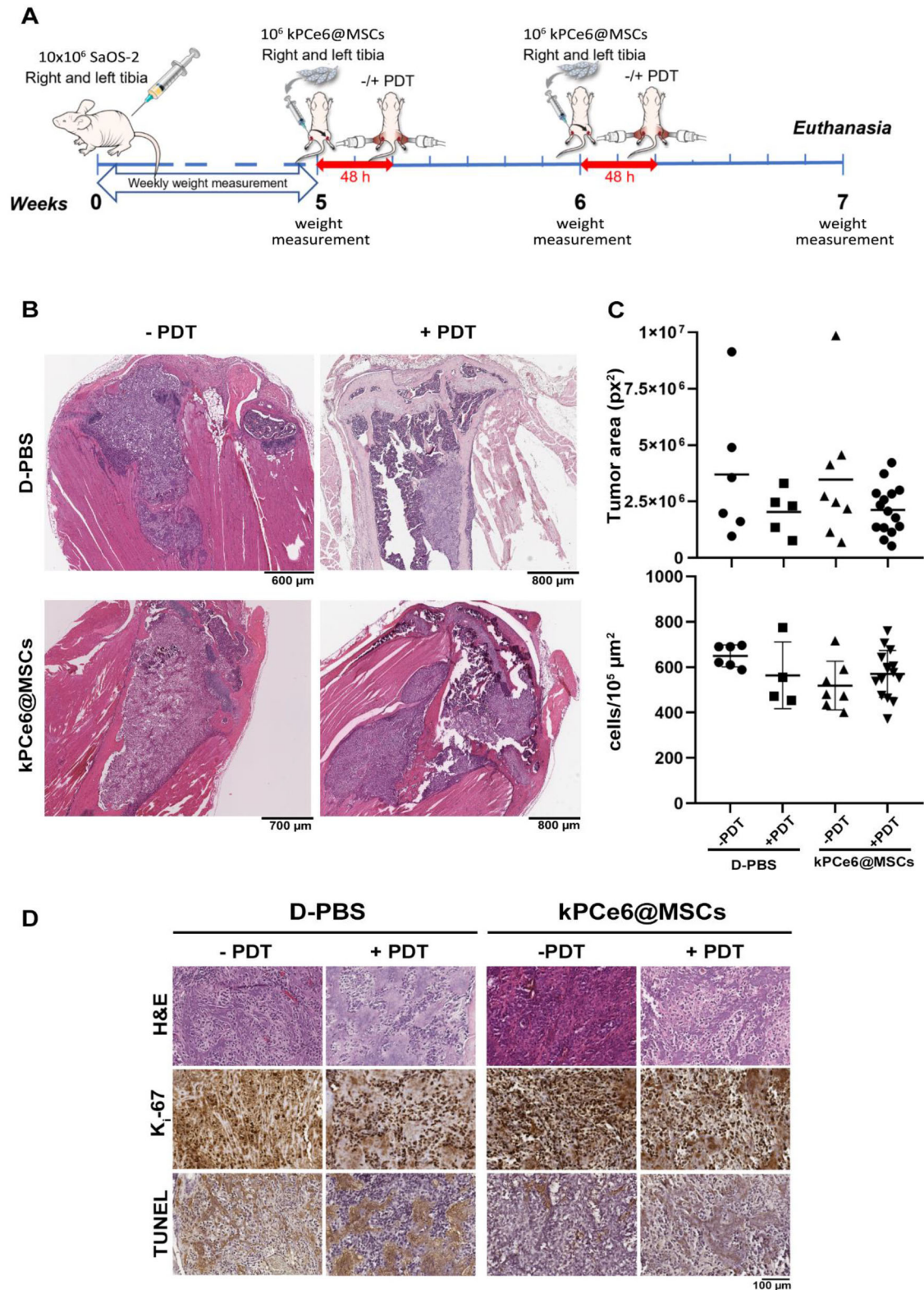


**Figure 7.** Preclinical evaluation: efficacy of kPCe6@MSCs in orthotopic murine OS model. A) Schematic representation of the workflow of the in vivo experimentation; B) Representative H&E-stained paraffin sections from tibia explants of animals from control groups (D-PBS  $-/+$  PDT) and treatment groups (kPCe6@MSCs  $-/+$  PDT). C) The graphs show the quantification of tumor area and tumor cell number, respectively, performed with QuPath software. Data are expressed as the mean  $\pm$  SD. D) Representative paraffin sections from tibia explants of animal kPCe6@MSCs from control groups (D-PBS  $-/+$  PDT) and treatment groups (kPCe6@MSCs  $-/+$  PDT) stained with the following markers: H&E, K<sub>i</sub>-67 and TUNEL.

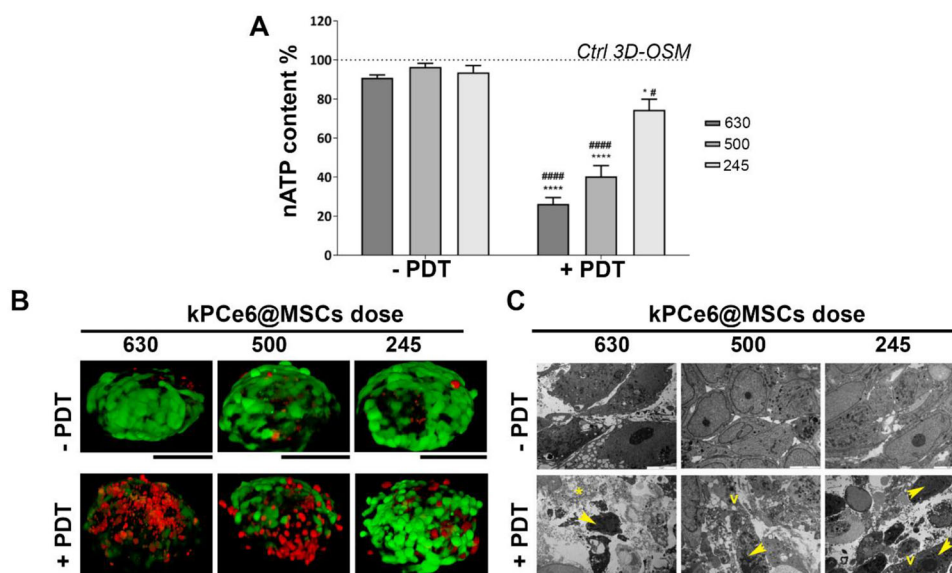


**Figure 8.** Numbers matter: Cell dose response in a 3D-OSM. A) The graph shows the Cell Titer Glo assay performed 24 h after irradiation (–/+PDT) at three different doses of kPCe6@MSCs (630, 500 and 245 cells) keeping fixed the number of MG-63 cells. The results are normalized to the corresponding 3D-OSM generated with unloaded MSCs and nonirradiated. Data, performed by GraphPad Prism 8 software, are expressed as mean ± SD ( $N = 6$  and  $n = 4$ ) and statistical analysis has been generated using the 2-way ANOVA test, and Tukey's multiple comparison test as a post-test. Results were considered statistically significant at  $p$  values < 0.05 (\* $p$ -values < 0.05, \*\* $p$ -values < 0.01, \*\*\* $p$ -values < 0.001, and \*\*\*\* $p$ -values < 0.0001). Data compared to respective unloaded MSCs are reported as \*, while the # indicate the statistical analysis performed comparing the corresponding ratio groups –/+PDT; B) Representative confocal images of Live&Dead staining (green Calcein AM staining of live cells and red EthD-1 staining of dead cells' nuclei) of nonirradiated (–PDT) and irradiated (+PDT) spheroids at different kPCe6@MSC doses. Scale bar 100  $\mu$ m. C) Representative TEM images of nonirradiated (–PDT) and irradiated (+PDT) spheroids at different kPCe6@MSC doses. Asterisks, V, and arrow heads highlight necrosis, cytoplasmic vacuolization, and chromatin clumping, respectively. Scale bar 5  $\mu$ m.

(arrow heads) was observed. The results obtained in the OS 3D in vitro model prove a cell-dose response as a critical parameter to be considered for preclinical and clinical applications.

### 3. Conclusion

In this study, we investigated crucial aspects of the MSCs-based delivery strategy, including uptake and retention ability, as well as cell migration capability when loaded with kPCe6 NPs. Although the in vitro results showed promise, the impact observed in an orthotopic preclinical murine OS model was negligible. This prompted us to explore the relationship between cell dosage and antitumor response in a 3D OS in vitro system, before proceeding with additional preclinical in vivo validation.

The outcomes obtained from the 3D model emphasized the significance of the number of kPCe6@MSCs utilized for treatment. Our findings strongly suggest that to achieve a tumor reduction exceeding 90%, it is necessary to inject a number of kPCe6@MSCs that is approximately 35% of the total tumor mass.

Considering that OS is often diagnosed at an advanced stage with a large tumor volume, our results indicate that employing kPCe6@MSCs for primary OS tumor eradication poses challenges, including the production of a substantial number of cells under Good Manufacturing Practices (GMP), which is currently costly and difficult to achieve with available technologies.

Up until June 2021, over a thousand clinical trials incorporating MSCs-based cell therapies for various diseases had been

registered globally. However, only a limited number, less than a dozen, have obtained global marketing authorization.<sup>[42]</sup> This gap is reasonably explained by the challenges and the costs posed by cell expansion protocols and standardization procedures.

Despite our evidence supporting that kPCe6@MSCs are not a sustainable option to treat OS primary tumors, kPCe6@MSCs could represent a valuable approach when the number of OS cells is limited, such as in case of small OS lung metastases or when the remaining tissue after surgical excision needs to be further cleared to reduce OS recurrence.

In conclusion, our work has defined important aspects related to MSCs as cellular vehicles of drugs loaded nanoformulations, possibly inspiring other researchers to pursue this therapeutic approach under different conditions.

### 4. Experimental Section

**Reagents:** Mc Coy's medium, Dulbecco's Modified Eagle's Medium – High Glucose (DMEM-HG), Dulbecco's modified Phosphate buffer solution (D-PBS), TryPLE select, Fetal Bovine Serum (FBS), Gluta-MAX, penicillin/streptomycin (P/S), TUNEL assay kit, Hoechst 33342, LIVE/DEAD, ProLong Diamond Antifade Mountant, were purchased by Life Technologies-Thermo Fisher Scientific (Waltham, MA USA).

Paclitaxel was purchased by TCI-Europe (Zwijndrecht, Belgium). Chlorin-e6 was purchased from Livchem Logistics GmbH (Frankfurt am Main, Germany).

**Isolation, Expansion, and Characterization of Human Mesenchymal Stromal Cells (MSCs):** Human MSCs have been isolated from BM samples

obtained from five different patients undergoing surgery at Rizzoli Orthopedic Institute (Bologna, Italy), after patient's informed consent, according to the protocol approved by the local ethical committee (n.0029817/2015, 03<sup>rd</sup> September 2015). BM aspirate was diluted one to one using D-PBS, and 4 mL were stratified on 3 mL of Ficoll Paque 1.078 g mL<sup>-1</sup> (GE-healthcare, Chicago, Illinois, USA). After the centrifugation, plasma and mononuclear cells were transferred to a new tube, and cells were counted using nucleocounter device (Chemometec, Allerod, Denmark). Mononuclear cells were then seeded in plastic flasks (Corning, Glendale, Arizona, USA) at a density of  $4 \times 10^5$  cells cm<sup>-2</sup>, changing medium twice a week up to 70% confluency. MSCs were expanded in complete medium (CM), consisting of  $\alpha$ -MEM (Lonza Group LTD, Basel, CH) supplemented with 20% of fetal bovine serum (FBS) and 1% GlutaMax. At 60–70% confluency, cells were washed once with D-PBS and then detached using TryPLE Select for 3 min at 37%. The cellular suspension was centrifuged at 1500 rpm for 3 min, and the cell pellet was resuspended in CM and counted using nucleocounter device (Chemometec, DN). The cells were seeded at  $2 \times 10^3$  cells cm<sup>-2</sup> density and expanded until passage 10. Cells at passages p3–p6 were used for all experiments.

Complete characterization in terms of proliferation rate (growth curve), fibroblast-colony forming unit (CFU) efficiency, immunophenotypic profile, and trilineage-differentiation potential of each MSCs line was performed as indicated in our previous study.<sup>[21]</sup>

Statistical parameters (median 25<sup>th</sup> and 75<sup>th</sup> percentiles), originating from the lab's database of characterization data from 28 MSCs lines, were used as criteria to set a score system for expansion and differentiation performances of the five MSCs isolated lines: 0 points for results below the 5<sup>th</sup> percentile, 2 points for results between the 5<sup>th</sup> percentile and the 25<sup>th</sup>, 4 points for results between 25<sup>th</sup> percentile and the median, 6 points for results between the median and the 75<sup>th</sup> percentile, 8 points for results between the 75<sup>th</sup> percentile and the 95<sup>th</sup> percentile, and 10 points for results above the 95<sup>th</sup> percentile. Additionally, an immunophenotype score (1 point for each positive CD $\geq$ 95% or negative CD $\leq$ 5%) was set to obtain a cumulative score system to rank the quality of the isolated MSCs lines.

**Human OS Cell Lines:** In the present work, two different oOS cell lines, purchased from ATCC (Manassas, VA, USA), were used: MG-63 for in vitro experiments and Saos-2 for orthotopic murine OS model.

MG-63 (ATCC-CRL-1427) were cultured in DMEM-HG supplemented with 10% FBS and 1% GlutaMAX. The medium was changed twice a week, and when cells reached 60–70% of confluence, they were expanded for further passaging.

Saos-2 (HTB-85) were cultured in McCoy's medium containing 15% of FBS and 1% GlutaMAX at 37 °C in a humidified atmosphere with 5% CO<sub>2</sub>. The medium was changed twice a week, and when cells reached 70–80% of confluence, they were expanded for further passaging.

**Preparation and Characterization of kPCe6 NPs:** kPCe6 NPs were obtained by the drug-induced aggregation method as previously described.<sup>[10,11]</sup> Briefly, a PBS solution of keratin covalently functionalized with Ce6, e.g. ker-Ce6,<sup>[43]</sup> and pristine keratin was prepared to a final Ce6 concentration of 40  $\mu$ g mg<sub>ker</sub><sup>-1</sup> and a final keratin concentration of 5 mg mL<sup>-1</sup>. A solution of PTX (10% w<sub>PTX</sub>/w<sub>ker</sub>) in ethanol (10 mg mL<sup>-1</sup>) was then slowly added (0.3 mL min<sup>-1</sup>) via a syringe pump under vigorous stirring (600 rpm). The solution was then stirred for 1 h, checked by dynamic light scattering, and lyophilized to obtain a powder of kPCe6.

kPCe6 NPs were characterized in terms of hydrodynamic diameter and zeta potential using a NanoBrook Omni Particle Size Analyzer (Brookhaven Instruments Corporation, New York, NY, USA) equipped with a 35 mW red diode laser (nominal 640 nm wavelength).

**Cytotoxicity Assay:** MSCs were seeded in a 96-well plate in complete medium at the concentration of  $5 \times 10^3$  cells per well and left to adhere overnight. The following day, medium was replaced with  $\alpha$ -MEM + 0.2% BSA supplemented with increasing concentration of kPCe6 ([PTX]<sub>equ</sub>: 0.5 pg mL<sup>-1</sup> – 50  $\mu$ g mL<sup>-1</sup>) for 72 h. In the end, the medium was removed, the monolayer culture was washed twice with D-PBS, and cell viability was assessed using WST-1 assay (Roche, Basel, CH) following the manufacturer protocol. Briefly, a working solution of complete medium supplemented with 10% WST-1 was made, and 100  $\mu$ L of the obtained solution was added

to each well. The plate was incubated for 2 h at 37 °C at 5% CO<sub>2</sub>, then the optical density of each well was measured by a microplate reader (Synergy HT, BioTek Winooski, VT, USA) set at 450 nm with the correction wavelength set at 690 nm.

**MSCs Loading with kPCe6 NPs:** MSCs were seeded in complete medium on multiwell plates at the density of  $1.6\text{--}2 \times 10^4$  cells cm<sup>-2</sup> to allow cell attachment. The day after, kPCe6 NPs were dissolved in H<sub>2</sub>O and sonicated for 5 min to improve their uniform dispersion. After medium removal, the cell monolayer was washed twice with D-PBS and kPCe6 NPs, diluted at a concentration of [PTX]<sub>equ</sub> = 5  $\mu$ g mL<sup>-1</sup> (corresponding to a [NPs] = 38.46  $\mu$ g mL<sup>-1</sup> and [Ce6] = 2.5  $\mu$ g mL<sup>-1</sup>) in  $\alpha$ -MEM supplemented with 0.2% Bovine Serum Albumin (BSA, Merck Millipore, Darmstadt, Germany), or 20% FBS (Figure S1, Supporting Information) were added. After 24 h in the dark at 37 °C and 5% CO<sub>2</sub> (loading phase), the medium was removed, and cells were gently washed three times with D-PBS, followed by replenishing with fresh medium.

After NPs exposure, kPCe6@MSCs were gently washed with D-PBS, detached using TryPLE Select for 3 min at 37 °C, and centrifuged at 1500 rpm for 3 min. Cell pellets were resuspended in a small amount of medium and Ce6 fluorescence intensity ( $\lambda_{Ex}$  662 nm,  $\lambda_{Em}$  668 nm, in ethanol) was measured using the automated cell counter Countess II FL (Life Technologies-Thermo Fisher Scientific, Waltham, MA USA) equipped with EVOS light cube CY5.5 (Ex: 655/46 nm; Em: 794/160 nm).

**Intracellular Localization:** Intracellular localization of keratin-based NPs was evaluated over time by seeding MSCs at  $1.6 \times 10^4$  cells cm<sup>-2</sup> density on a glass Petri dish (Ibidi GmGH, Gräfelfing, Germany) in complete medium and let to adhere o/n. The following day, the medium was replaced with  $\alpha$ -MEM + 0.2% BSA and kPCe6 NPs at [PTX]<sub>equ</sub> 5  $\mu$ g mL<sup>-1</sup> for 24 h. At the end of loading time, the medium was removed, the cell monolayer washed twice with D-PBS, and new complete medium was added. At each time point (end of loading, 0, 2, and 6 days after loading), media was replaced with new CM supplemented with  $100 \times 10^{-9}$  M of lysotracker DND26 (Thermo Fisher Scientific) and  $8.12 \times 10^{-6}$  M of Hoechst 33342 (Thermo Fisher Scientific), incubated at 37 °C for 10 min, and the samples were analyzed. Images were taken at high magnification with a NIKON A1-R confocal laser scanning microscope equipped with a NIKON Plan Apo 60 $\times$  oil DIC N2, 1.4 NA objective lens, and 405, 488, and 646 nm laser lines to excite Hoechst (405 nm), DND26 (488 nm), and Chlorin e6 (646 nm) fluorescence signals. The emission signals were detected by a photomultiplier tube (DU4) preceded by emission filters BP 450/50, 525/50 nm, and BP 595/50 nm for Hoechst, DND26, and Chlorin e6, respectively.

Three different confocal images for each time point were used for the colocalization analysis of Ce6 over Lysotracker DND-26. The analysis was performed using the Fiji/ImageJ Colocalization Threshold plug-in, and Pearson's correlation coefficient values were generated and used for the statistical analysis.

**In Vitro Migration Assays:** Transwell assay: The migration of unloaded MSCs and kPCe6@MSCs was assessed using the Boyden chamber technique. Cell culture inserts for a 24-well plate with 8  $\mu$ m pore diameter were used (Millipore, Darmstadt, Germany). An aliquot of  $1.5 \times 10^4$  unloaded or kPCe6@MSCs was resuspended in 100  $\mu$ L of  $\alpha$ -MEM with 0.2% BSA and placed in the upper part of the Boyden chamber. The lower well was filled with 600  $\mu$ L of  $\alpha$ -MEM + 0.2% BSA, as negative ctrl, or  $\alpha$ -MEM + 20% FBS (positive ctrl) or MG-63 CM (MG-63 CM), known as two distinct chemo-attractant solutions. After overnight incubation, the medium in the lower chamber was discarded, and the cells at the bottom of the membrane were fixed in methanol for 5 min at RT, then Hema 3 kit staining was used to stain cells according to the manufacturer's instruction (Fisher HealthCare, Thermo Fisher Scientific). For each sample, 10 images were acquired at 20 $\times$  objective using an inverted Nikon Eclipse TE2000-U microscope (Nikon, Amsterdam, The Netherlands), and cell nuclei were counted by two independent researchers and averaged. All experiments were performed in triplicates.

To prepare the CM, MG-63 were seeded in DMEM-10% FBS on flasks and grown until 80–90% of confluence; then, the medium was discarded, cell monolayer washed twice with D-PBS to remove all serum residues, and the medium was replaced with DMEM-HG supplemented with 0.2%

BSA for 72 h. At the end medium was collected, centrifuged at 1500 rpm for 3 min to eliminate all cell debris, and stored at  $-30^{\circ}\text{C}$  until use.

**Scratch assay:** For the scratch assay, unloaded and kPCE6@MSCs were seeded at the density of  $7.5 \times 10^3$  cell  $\text{cm}^{-2}$  inside both wells of the Ibidi inserts (Culture-insert 2 well, Ibidi GmgH) and let adhere overnight. The day after, the medium was removed, cell monolayer was washed twice with D-PBS to remove all serum traces, and the medium ( $\alpha$ -MEM+0.2% BSA) supplemented with kPCE6 NPs ( $[\text{PTX}]_{\text{equ}} 5 \mu\text{g mL}^{-1}$ ), was added for 24 h. At the end of the loading phase, the medium was removed, the cells were washed with D-PBS, and the IBIDI inserts were discarded. Images were acquired at time 0 and after 18, 24 and 48 h. Images were taken using a 4x objective lens and analyzed using Fiji/ImageJ by calculating the empty wound area (scratched area) at different time points, converting then the pixel area in percentage normalized to the time 0 (100%) of the control condition (unloaded MSCs).

**In Vivo Experimentation and Analyses:** Animals were housed according to the D.L.vo 26/2014, Directive 2010/63/EU, for the protection of animals used for scientific purposes and 2007/526/EC (recommendation for the accommodation and care of animals used for experimental and other scientific purposes). All animal operations were approved by the local Ethical Committee (00 24712/2015, 9<sup>th</sup> July 2015) and by the Animal Welfare Body (30<sup>th</sup> July 2015) of IRCCS Istituto Ortopedico Rizzoli and authorized by the Italian Ministry of Health (1271/2015-PR, 15<sup>th</sup> December 2015). The orthotopic murine OS model was developed in six-week-old male nude mice (BALB/c, nu/nu; Envigo RMS S.r.l., Azzida San Pietro Natisone, Udine, Italia) as previously described.<sup>[11]</sup> Briefly, an 18 G needle aligned perpendicularly to the tibial plate was introduced bending the knee of each nude mouse to  $90^{\circ}$  to reach the medullar channel and used as trocar for the Hamilton syringe loaded with a 26 G needle to inject  $10 \times 10^6$  Saos-2 cells resuspended in 50  $\mu\text{L}$  of D-PBS. Tumor was induced on both tibias. Animal weight measurement was performed and recorded weekly; animal clinical conditions were checked daily to monitor their wellbeing. For the efficacy study, 34 mice were used: 13 animals in the control group and 21 in the treatment group. After 5 weeks from the tumor inoculation, the animals included in the treatment groups were treated with  $10^6$  kPCE6@MSCs, previously resuspended in 50  $\mu\text{L}$  of D-PBS, inoculated with an insulin syringe by two small shots close to the tibia's proximal epiphysis. Forty-eight hours after treatment, half of the treated animals were exposed to LED light irradiation (irradiated group, + PDT). A LED device was designed and manufactured in-house as previously described.<sup>[11]</sup> Briefly, the device is equipped with LED lights (LZ4-00R208 Deep Red,  $660 \pm 2$  nm; 6.6 W; light intensity  $93.3$  mW  $\text{cm}^{-2}$  at 670 nm, Mouser Electronics, Mansfield, TX, USA) topped with two heating dissipators and two black cylinders to focus the light on the hind leg's area and spare the rest of the body. In the in vivo experimentation, the tumor bearing area was irradiated for 15 min keeping the LED light at 1 cm distance from the bottom of the cylinders to the skin of the mouse leg (Fluence:  $84$  J  $\text{cm}^{-2}$ ).

All operations, such as cell inoculation and PDT, were performed under general anesthesia. The anesthesia was induced and maintained with a mixture of  $\text{O}_2$ /air and isoflurane (2–3%) in spontaneous ventilation using an induction box and a facial mask and keeping the animals on a warm pad to avoid hypothermia during the procedures.

**Histological Analyses:** At the end of experimental time, the animals were premedicated with intramuscular Rompun (xylazine) injection and then euthanized by intracardiac Tanax (MSD Animal Health S.r.l., Segrate, Milano, Italy). Tibia explants were collected and fixed for 24 h in 4% paraformaldehyde, then decalcified in a 4% EDTA solution for 7 days at RT, changing the solution after 3 days, paraffin embedded, and processed.<sup>[11]</sup>

Paraffin blocks were sliced with a sledge microtome in 5  $\mu\text{m}$  thickness slice, following the tibias longitudinal plane in order include the entire tibia length. Slices were mounted onto Poly-lysine glass slides and stained with Hematoxylin & Eosin (H&E) according to the anatomical histopathology service protocol used (IFOM facility, Milan). H&E slides of all tumors were reviewed with the help of an expert pathologist, and the histological diagnosis was confirmed according to standardized criteria for OS identification.<sup>[4]</sup> Tumor area quantification was performed by manual selection from two operators in every H&E image. On the same images, the cell quantification was performed by selecting five different ROIs of  $10^5$

$\mu\text{m}^2$  area within the entire tumor area region, then the nuclei were manually counted using QuPath.<sup>[44]</sup> The obtained results were averaged and plotted.

**TUNEL assay** (Click-iT Tunel colorimetric IHC detection kit) was performed according to the manufacturer's protocol with the following minor modifications: proteinase K incubation was settled at 20 min at RT and the DAB reaction mixture incubation was defined at 15 min.

For immunohistochemical analysis, unstained sections were heat-treated at  $60^{\circ}\text{C}$  for 20 min, deparaffinized, and immunostained on a Ventana BenchMark following the manufacturer's guidelines (Ventana Medical Systems, Tucson, AZ, USA). To analyze the expression of  $\text{K}_i$ -67, immunostaining using a  $\text{K}_i$ -67 rabbit monoclonal primary antibody (clone 30–9; Ventana) and Avidin–biotin complex peroxidase was performed. All images were acquired using Aperio Digital Pathology Slide Scanner (Leica Biosystems, Milano, Italy).

**Confocal Laser Scanning Microscopy and Fluorescent Lifetime Imaging:** Paraffin-embedded slices were treated as previously described.<sup>[11]</sup> Fluorescence confocal imaging was performed with a confocal fluorescence microscope Nikon A1 (Nikon Co., Shinjuku, Japan) equipped with an Argon ion CW laser, a 640 nm CW diode laser, 405 nm and 640 nm pulsed/CW diode lasers (PicoQuant GmbH, Berlin, Germany). Images were collected using either a Nikon Plan Apo VC 20X air objective with NA 0.8 or a Nikon Plan Apo VC 60X oil immersion objective with NA 1.40. Filters were set to register the fluorescence in the 460–500 nm, 510–540 nm, 555–615 nm, and 665–735 nm ranges. The Nikon A1 spectral module with a precisely corrected 32-PMT array detector was used for spectral imaging. Wavelength resolution was set to 6 nm per PMT.

FLIM was performed as previously described,<sup>[11]</sup> exciting samples with the pulsed 405 nm diode laser and collecting photons at 655 nm/40 and with integrated PicoHarp 300 electronics (PicoQuant GmbH) for time-correlated single photon counting (TCSPC) measurements. The contribution of Hoechst excitation at 405 nm is negligible at the 635–675 nm emission range and can be separated from Ce6 emission. Hoechst has an average fluorescence lifetime of 2.1 ns (measured in the 460–500 nm range) in the tissues.

The fluorescence decay profile was analyzed with a least-squares method, using bi- or tri-exponential decay functions provided by Picoquant SymPho-Time software. Calculated Instrumental Response Function was used for deconvolution. The average fluorescence lifetime image was calculated by fixing the lifetimes obtained from the analysis of the histogram of the region of interest while the software calculates the preexponential factors for each pixel.

The fitting function used is:

$$I(t) = b + \sum_j a_j e^{-t/\tau_j} \quad (1)$$

The fractional intensity and the average fluorescence lifetime are calculated according to the following equations:

$$f_i = a_i \tau_i / \sum_j a_j \tau_j \quad (2)$$

$$\tau_{av} = \sum_j f_j \tau_j \quad (3)$$

**In Vitro 3D-Scaffold-Free OS Model:** The 3D scaffold-free OS model defined as 3D-OSM was generated by mixing different cell number of unloaded MSCs or kPCE6@MSCs (3170, 1360, 630, 500, 245), with the MG63 number fixed at 9500/100  $\mu\text{L}$  (which correspond to the following ratio 1:3, 1:7, 1:15, 1:19, and 1:39). The cell suspension was then dispensed in an ultralow attachment U-bottom 96-well plate, 100  $\mu\text{L}$  per well (Corning Costar, Amsterdam, The Netherlands). The day after 100  $\mu\text{L}$  per well of in DMEM-HG + 10% FBS was added and allowed to aggregate for 4 days.

In vitro experiments, 3D-OSMs were irradiated for 10 min using a LED light source ( $\lambda_{\text{max}} = 668 \pm 3$  nm) at room temperature, placing light-emitting source directly under the tissue culture plates (see Figure 7A, light intensity:  $198$  mW  $\text{cm}^{-2}$ ; fluence:  $120$  J  $\text{cm}^{-2}$ ).

Evaluation of PTX effect: The day after 3D-OSM creation and for the following 4 days, at least five spheroids per condition has been used to evaluate the cytotoxic effect of PTX using CellTiter-Glo 3D (Promega Corporation, Madison, Wisconsin, USA), an ATP content-based assay, following the manufacturer's protocol.

Evaluation of PTX and PDT effect: after 4 days from 3D-OSM generation, the medium was replaced, 3D-OSM moved on an ultra-low attachment 48-well plate, and half of them photoactivated with a LED source ( $667 \pm 3$  nm) for 10 min at RT (for details see 2.11 PDT treatments) and left at  $37^\circ\text{C}$  5%  $\text{CO}_2$  for 24 h. Cell death was evaluated through CellTiter-Glo 3D (Promega Corporation), an ATP content-based assay, following the manufacturer's protocol. Additionally, a LIVE/DEAD (Life Technologies) staining was performed according to the following protocol: the 3D-OSM were incubated with  $2.5 \times 10^{-6}$  M Calcein-AM in DMEM Phenol Red-free for 2 h first, then ethidium homodimer-1 (EthD-1) was added to a  $5 \times 10^{-6}$  M final concentration for 10 min. Z-stacks images, for a total depth of 100–120  $\mu\text{m}$ , were acquired with an A1R confocal laser scanner (Nikon, Amsterdam, The Netherlands) using Nikon Plan Apo VC 20x/0.75 NA DIC N2 objective lens and 3D rendering was performed with NIS elements software using the Alpha-blending algorithm.

**TEM Analysis:** 3D-OSM samples were fixed with 2.5% glutaraldehyde in 0.1 M cacodylate pH 7.6 buffer for 1 h at room temperature. After post-fixation with 1%  $\text{OsO}_4$  in cacodylate buffer for 1 h, samples were dehydrated in an ethanol series and embedded in Epon resin. Ultrathin sections (70 nm) were cut using an ultramicrotome and contrasted with uranyl acetate and lead citrate and observed with a Jeol Jem-1011 transmission electron microscope (Jeol Jem, USA).

**Statistical Analysis:** Data presented in this manuscript are expressed as mean  $\pm$  S.D. In specific conditions, raw data are normalized versus controls, e.g., unloaded or untreated cells, as reported in the corresponding legend figure. Results were obtained from at least three independent experiments ( $N = 3$ ), and each experiment was performed at least in triplicate ( $n = 3$ ) unless otherwise stated in figure legend.

Unpaired *t*-test was used to analyze 2D results (Figures 2D,E and 3D and Figure S1, Supporting Information) and they were statistically significant at *p* values  $< 0.05$ . \**p*-values  $< 0.05$ , \*\**p*-values  $< 0.01$ , \*\*\**p*-values  $< 0.001$ , \*\*\*\**p*-values  $< 0.0001$ .

Two-way ANOVA followed by Tukey's multiple comparisons test was applied to analyze all data resulting from the 3D-OSM model. Results were statistically significant at *p*-values  $< 0.05$ . The statistical analysis was performed with GraphPad Prism 8 Software (GraphPad; San Diego, CA, USA).

## Supporting Information

Supporting Information is available from the Wiley Online Library or from the author.

## Acknowledgements

The authors are sincerely grateful to the staff of the Scienze e tecnologia chirurgiche, IRCCS Istituto Ortopedico Rizzoli, particularly to Nicolò Nicoli Aldini, who performed the intratibial injections. The authors wish to thank Silvano Favaretto and Giorgio Longino ISOF-CNR for the development of the prototype device for in vivo photodynamic therapy; Maria Pia Cumani-University of Bologna for the graphical abstract; Federica Pisati, manager of Cogentech histopathology service-IFOM, Milan (Italy) for the help in the sectioning of histological samples, Arnleto Fiocchi, team member of the Animal Histopathology facility-CAST Center San Raffaele Hospital, Milan (Italy) for Aperio imaging acquisition. The authors wish to thank Dr Carmine Onofrillo, Dept. of Surgery University of Melbourne, for the critical revision of the manuscript and Jorge Melendez, undergraduate student in biomedical engineering at Northwestern University (Evanston, IL; USA) for English language editing. This research was funded by the My First Airc Grant of the Italian Association for Cancer Research, grant number MFAG-16941 to S.D.

Open access publishing facilitated by The University of Melbourne, as part of the Wiley - The University of Melbourne agreement via the Council of Australian University Librarians.

## Conflict of Interest

The authors declare no conflict of interest.

## Data Availability Statement

The data that support the findings of this study are available from the corresponding author upon reasonable request.

## Keywords

cells-based drug delivery, keratin nanoparticles, mesenchymal stromal cells, osteosarcoma, photodynamic therapy

Received: February 7, 2023

Revised: May 22, 2023

Published online: July 11, 2023

- [1] A. Misaghi, A. Goldin, M. Awad, A. A. Kulidjian, *SICOT-J* **2018**, 4, 12.
- [2] G. Ottaviani, N. Jaffe, *Cancer Treat. Res.* **2009**, 152, 3.
- [3] C. M. Hattinger, M. P. Patrizio, F. Magagnoli, S. Luppi, M. Serra, *Expert Opin. Emerging Drugs* **2019**, 24, 153.
- [4] V. D. S., P. Picci, (Eds: P. Picci, M. Manfrini, N. Fabbri, M. Gambarotti), *Atlas of Musculoskeletal Tumors and Tumorlike Lesions*, Springer International Publishing, Cham, Switzerland **2014**.
- [5] S. Ferrari, M. Serra, *Expert Opin. Pharmacother.* **2015**, 16, 2727.
- [6] C. M. Hattinger, M. Pasello, S. Ferrari, P. Picci, M. Serra, *Expert Opin. Emerging Drugs* **2010**, 15, 615.
- [7] S. Ferrari, A. Briccoli, M. Mercuri, F. Bertoni, M. Cesari, A. Longhi, G. Bacci, *J. Pediatr. Hematol. Oncol.* **2006**, 28, 418.
- [8] S. R. Patel, N. E. Papadopoulos, C. Plager, K. A. Linke, S. H. Moseley, C. H. Spiridonidis, R. Benjamin, *Cancer* **1996**, 78, 741.
- [9] L. Amoroso, V. Castel, G. Bisogno, M. Casanova, C. Marquez-Vega, J. C. Chisholm, F. Doz, L. Moreno, A. Ruggiero, N. U. Gerber, F. Fagioli, P. Hingorani, S. G. Melcón, R. Slepets, N. Chen, Y. Le Bruchec, M. Simcock, G. Vassal, *Eur. J. Cancer* **2020**, 135, 89.
- [10] E. Martella, C. Ferroni, A. Guerrini, M. Ballestri, M. Columbaro, S. Santi, G. Sotgiu, M. Serra, D. M. Donati, E. Lucarelli, G. Varchi, S. Duchi, *Int. J. Mol. Sci.* **2018**, 19, 3670.
- [11] E. Martella, B. Dozza, C. Ferroni, C. O. Obeyok, A. Guerrini, D. Tedesco, I. Manet, G. Sotgiu, M. Columbaro, M. Ballestri, L. Martini, M. Fini, E. Lucarelli, G. Varchi, S. Duchi, *Pharmaceutics* **2022**, 14, 677.
- [12] Y. Takayama, K. Kusamori, M. Nishikawa, *Expert Opin. Drug Delivery* **2021**, 18, 1627.
- [13] T. Zhang, R. Lin, H. Wu, X. Jiang, J. Gao, *Adv. Drug Delivery Rev.* **2022**, 185, 114300.
- [14] A. Hassanzadeh, A. H. Altajer, H. S. Rahman, M. M. Saleh, D. O. Bokov, W. K. Abdelbasset, F. Marofi, M. Zamani, Y. Yaghoubi, M. Yazdanifar, Y. Pathak, M. S. Chartrand, M. Jarahian, *Front. Cell Dev. Biol.* **2021**, 9, 686453.
- [15] M. Studeny, F. C. Marini, R. E. Champlin, C. Zompetta, I. J. Fidler, M. Andreeff, *Cancer Res.* **2002**, 62, 3603.
- [16] S. Duchi, G. Sotgiu, E. Lucarelli, M. Ballestri, B. Dozza, S. Santi, A. Guerrini, P. Dambrosio, S. Giannini, D. Donati, C. Ferroni, G. Varchi, *J. Controlled Release* **2013**, 168, 225.

- [17] Y. Zheng, G. Wang, R. Chen, Y. Hua, Z. Cai, *Stem Cell Res. Ther.* **2018**, 9, 22.
- [18] X. Ouyang, X. Wang, H.-B. Kraatz, S. Ahmadi, J. Gao, Y. Lv, X. Sun, Y. Huang, *Biomater. Sci.* **2020**, 8, 1160.
- [19] G. Grisendi, C. Spano, N. D'souza, V. Rasini, E. Veronesi, M. Prapa, T. Petrachi, S. Piccinno, F. Rossignoli, J. S. Burns, S. Fiorcari, D. Granchi, N. Baldini, E. M. Horwitz, V. Guarneri, P. Conte, P. Paolucci, M. Dominici, *Stem Cells* **2015**, 33, 859.
- [20] B. Qiao, W. Shui, L. Cai, S. Guo, D. Jiang, *Drug Des., Dev. Ther.* **2015**, 9, 969.
- [21] S. Lenna, C. Bellotti, S. Duchi, E. Martella, M. Columbaro, B. Dozza, M. Ballestri, A. Guerrini, G. Sotgiu, T. Frisoni, L. Cevolani, G. Varchi, M. Ferrari, D. M. Donati, E. Lucarelli, *J. Exp. Clin. Cancer Res.* **2020**, 39, 40.
- [22] M. Pierini, C. Di Bella, B. Dozza, T. Frisoni, E. Martella, C. Bellotti, D. Remondini, E. Lucarelli, S. Giannini, D. Donati, *J. Bone Jt. Surg., Am. Vol.* **2013**, 95, 1101.
- [23] E. Martella, C. Bellotti, B. Dozza, S. Perrone, D. Donati, E. Lucarelli, *Cytotherapy* **2014**, 16, 1476.
- [24] M. Dominici, K. Le Blanc, I. Mueller, I. Slaper-Cortenbach, F. Marini, D. Krause, R. Deans, A. Keating, D. Prockop, E. Horwitz, *Cytotherapy* **2006**, 8, 315.
- [25] E. M. Horwitz, K. Le Blanc, M. Dominici, I. Mueller, I. Slaper-Cortenbach, F. C. Marini, R. J. Deans, D. S. Krause, A. Keating, *Cytotherapy* **2005**, 7, 393.
- [26] S. Viswanathan, Y. Shi, J. Galipeau, M. Krampera, K. Leblanc, I. Martin, J. Nolte, D. G. Phinney, L. Sensebe, *Cytotherapy* **2019**, 21, 1019.
- [27] J. A. Guadix, J. López-Beas, B. Clares, J. L. Soriano-Ruiz, J. L. Zugaza, P. Gálvez-Martín, *Pharmaceutics* **2019**, 11, 552.
- [28] C. Gottstein, G. Wu, B. J. Wong, J. A. Zasadzinski, *ACS Nano* **2013**, 7, 4933.
- [29] N. D. Donahue, H. Acar, S. Wilhelm, *Adv. Drug Delivery Rev.* **2019**, 143, 68.
- [30] T. Wongpinyochit, B. F. Johnston, F. P. Seib, *ACS Biomater. Sci. Eng.* **2018**, 4, 942.
- [31] B. Čunderlíková, L. Gangeskar, J. Moan, *J. Photochem. Photobiol., B* **1999**, 53, 81.
- [32] H. Fu, Y. Wu, X. Yang, S. Huang, F. Yu, H. Deng, S. Zhang, Q. Xiang, *All Life* **2021**, 14, 782.
- [33] A. L. Ponte, E. Marais, N. Gally, A. Langonné, B. Delorme, O. Hérault, P. Charbord, J. Domenech, *Stem Cells* **2007**, 25, 1737.
- [34] X. Xuan, C. Tian, M. Zhao, Y. Sun, C. Huang, *Cancer Cell Int.* **2021**, 21, 595.
- [35] F. Tang, Y. Tie, Y. Q. Wei, C. Q. Tu, X. W. Wei, *Biochim. Biophys. Acta, Rev. Cancer* **2021**, 1876, 188606.
- [36] M. E. Halkos, Z.-Q. Zhao, F. Kerendi, N.-P. Wang, R. Jiang, L. S. Schmarkey, B. J. Martin, A. A. Quyyumi, W. L. Few, H. Kin, R. A. Guyton, J. Vinten-Johansen, *Basic Res. Cardiol.* **2008**, 103, 525.
- [37] S. M. Hashemi, S. Ghods, F. D. Kolodgie, K. Parcham-Azad, M. Keane, D. Hamamdzcic, R. Young, M. K. Rippey, R. Virmani, H. Litt, R. L. Wilensky, *Eur. Heart J.* **2008**, 29, 251.
- [38] H. Hamamoto, J. H. Gorman, L. P. Ryan, R. Hinmon, T. P. Martens, M. D. Schuster, T. Plappert, M. Kiupel, M. G. St John-Sutton, S. Itescu, R. C. Gorman, *Ann. Thorac. Surg.* **2009**, 87, 794.
- [39] H. Zhang, Y. Feng, X. Xie, T. Song, G. Yang, Q. Su, T. Li, S. Li, C. Wu, F. You, Y. Liu, H. Yang, *Adv. Healthcare Mater.* **2022**, 11, 2101375.
- [40] T. E. G. Krueger, D. L. J. Thorek, S. R. Denmeade, J. T. Isaacs, W. N. Brennen, *Stem Cells Transl. Med.* **2018**, 7, 651.
- [41] H. L. Smith, S. A. Beers, J. C. Gray, J. M. Kanczler, *Int. J. Mol. Sci.* **2020**, 21, 5499.
- [42] D. Jovic, Y. Yu, D. Wang, K. Wang, H. Li, F. Xu, C. Liu, J. Liu, Y. Luo, *Stem Cell Rev. Rep.* **2022**, 18, 1525.
- [43] A. Aluigi, G. Sotgiu, C. Ferroni, S. Duchi, E. Lucarelli, C. Martini, T. Posati, A. Guerrini, M. Ballestri, F. Corticelli, G. Varchi, *RSC Adv.* **2016**, 6, 33910.
- [44] P. Bankhead, M. B. Loughrey, J. A. Fernández, Y. Dombrowski, D. G. McArt, P. D. Dunne, S. McQuaid, R. T. Gray, L. J. Murray, H. G. Coleman, J. A. James, M. Salto-Tellez, P. W. Hamilton, *Sci. Rep.* **2017**, 7, 16878.